Response dynamics of spiking network models to incoming seizure-like perturbation

Damien Depannemaecker, Mallory Carlu, Alain Destexhe

Manuscript Title

Response dynamics of spiking network models to incoming seizure-like perturbation

Abbreviated Title

Seizure-like propagation in spiking network models

List of all Authors Names and Affiliations

Damien Depannemaecker[1,*], Mallory Carlu[1,*], Alain Destexhe[1]
[1] Paris-Saclay University, French National Centre for Scientific Research (CNRS), Institute of Neuroscience (NeuroPSI), 91198 Gif sur Yvette, France
* equally contributing first authors

Author contribution

DD and MC performed the research, analyzed data and wrote the paper, contributing equally; DD, MC and AD designed research and revised the paper.

Corresponding author

Damien Depannemaecker
Paris-Saclay Institute of Neuroscience (NeuroPSI)
1, avenue de la Terrasse
91198 Gif sur Yvette, France
damien.d@cnrs.fr

Number of figures, tables, multimedia

number of figures: 8
number of table: 1
multimedia: 0

Number of words for abstract, introduction, and discussion

abstract: 202 words
significance : 72 words
introduction: 657 words
discussion: 1174 words

Conflicts of Interest

The authors declare no competing financial interests.

Acknowledgements / Funding information

This work was funded from the European Union's Horizon 2020 Framework Programme for Research and Innovation under the Specific Grant Agreement No. 945539 (Human Brain Project SGA3) and the Centre National de la Recherche Scientifique (CNRS, France).

Abstract

Epilepsies are characterized by electrophysiological crises in the brain, which were first observed thanks to electroencephalograms. However, it is known that seizures originating from one or more specific regions may or may not spread to the rest of the brain, while the exact mechanisms are unclear. We propose three computational models at the neural network scale to study the underlying dynamics of seizure propagation, understand which specific features play a role, and relate them to clinical or experimental observations. We consider both network features, such as the internal connectivity structure and single neuron model, and input properties in our characterization. We show that a paroxysmal input leads to a dynamical heterogeneity inside the network, non-trivially related with its architecture, which may or may not entrain it into a seizure. Although hard to anticipate because of the intricate nature of the instability involved, the seizure propagation might be circumvented upon acting on the network during a specific time window. As we deal with a complex system, which seems to depend non trivially on various parameters, we propose a probabilistic approach to the propagative/non-propagative scenarios, which may serve as a guide to control the seizure by using appropriate stimuli.

Significance: Our computational study shows the specific role that the inhibitory population can have and the possible dynamics regarding the propagation of seizure-like behavior in three different neuronal networks. The study conducts in this paper results from the combination of structural aspects and time-continuous measures, which helps us unravel the internal dynamics of the network. We show the existence of a specific time window favorable to the reversal of the seizure propagation.

1 Introduction

Epilepsy is one of the most common neurological diseases (Beghi, 2019), which can take numerous forms. It is associated with the presence of electrophysiological seizures, usually recorded in humans using electroencephalogram (EEG). However, EEG recordings do not allow us to probe the activity of each neuron within the network. More recently, the recording carried out with microelectrode arrays made it possible to obtain spike information of the order of a hundred neurons (Peyrache et al., 2012; Dehghani et al., 2016).

It has then been observed that the neuronal activity does not necessarily

correspond to synchronized spikes of the whole neuron population, as previously modeled (*Computational Neuroscience in Epilepsy*, 2008) and can be modeled at different scales from cellular to whole-brain levels(Depannemaecker, Destexhe, Jirsa, & Bernard, 2021; Depannemaecker et al., 2020). In fact, it turns out that the dynamics of neural networks during seizures are more complex (Jiruska et al., 2013), and the mechanisms of propagation at different scales are poorly understood.

We take as a starting point examples of seizures where the inhibitory network is strongly recruited, while excitatory cells' firing is diminished. Fig.1 shows three seizures from a patient who was recorded using Utah-arrays, before resection surgery in a case of untractable epilepsy. From these intracranial recordings, 92 neurons have been identified and isolated and were classified into two groups: Fast-Spiking (FS) neurons and Regular-Spiking (RS) neurons, based on spike shape, autocorrelograms, and firing rates (Peyrache et al., 2012). Remarkably, direct cell-to-cell functional interactions were observed, which demonstrated that some of the FS cells are inhibitory while some of the RS cells are excitatory (see details in (Peyrache et al., 2012)). The three seizures shown in Fig.1 were taken from the analysis of (Dehghani et al., 2016) (see this paper for details), and are shown with the firing rate of each population of cells. During the seizure, we can observe a plateau of high activity of FS cells, and a strongly reduced activity of RS cells. This phenomenon of unbalanced dynamics between RS and FS cells was only seen during seizures in this patient (Dehghani et al., 2016). It shows that, in these three examples, the seizure was manifested by a strong "control" by the inhibitory FS cells, which almost silenced excitatory RS cells. It is interesting to see that a very different conclusion would be reached if no discrimination between RS and FS cells was performed, which underlies the importance of recording inhibitory cells during seizures.

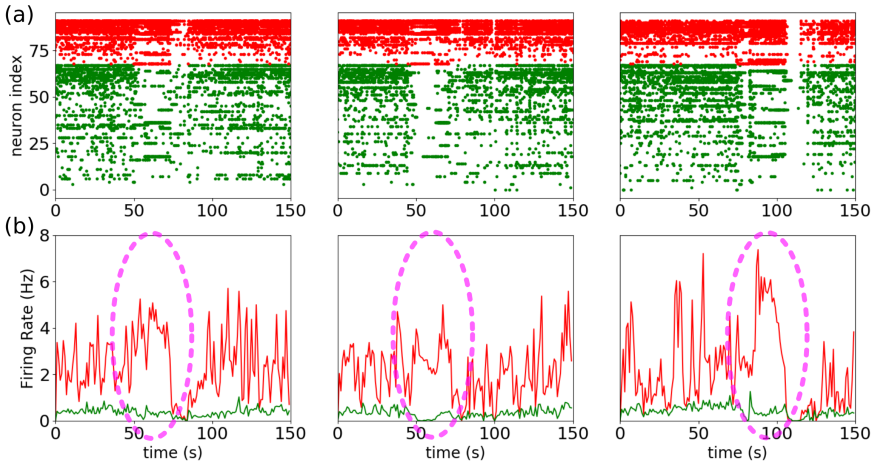

Figure 1: **Examples of inhibitory recruitment during seizures:** (a) Raster plot of three different seizures from the same patient, 92 neurones where identified 24 putatives inhibitory cells (red) and (68) putative excitatory cells (green) (b) Corresponding firing rate of the putative inhibitory population (red) and the putative excitatory population (green). A plateau of high activity of the putative inhibitory cells can be observed during the seizure (highlighted in dashed purple oval). Done with data from (Dehghani et al., 2016).

The region of the brain where the seizure starts is called the seizure focus, although in certain patients it is distributed over several foci (Nadler & Spencer, 2014), then the seizure spreads to other regions of the brain. When another such region is reached, it can in turn display a seizure, or manage to control it, thus preventing its spread to further regions.

In order to gain understanding on the dynamics underlying this type of mechanisms, we study the response of networks composed of three different neuron models (Adaptive exponential Integrate and fire (AdEx), Conductance-based Adaptive Exponential integrate-and-fire (CAdEx), and Hodgkin-Huxley (HH) models) interacting through conductance-based synapses, to an incoming paroxysmal (seizure-like) perturbation. We observe two types of behavior: one where the incoming perturbation transfers to the excitatory population, thus making its activity stronger than the input, and the other where only the inhibitory

population strongly increases its activity, thus controlling the perturbation. We then propose a more precise approach, based on the AdEx network, that mixes structural and dynamical ingredients in order to unravel key aspects of the mechanisms into play. Focusing on the different input connectivity profiles for each node in the network, we are able to build separate groups of neurons that display significantly different dynamics with respect to the perturbation. Finally, we study the possibility of a proactive approach, based on the application of an extra stimulus with the aim of reversing the propagative behavior.

2 Material and methods

2.1 Computational models

We use for this study a mathematical model of electrophysiological activity based on ordinary differential equations, describing the dynamics of the neuron's membrane potential through their interactions.

Each model of neuron of the network is described by the equation (13) of the Adaptative Exponential integrate and fire (AdEx) model (Naud, Marcille, Clopath, & Gerstner, 2008).

$$C\frac{dV}{dt} = g_L(E_L - V) + g_L\Delta_T \exp\left(\frac{V - V_T}{\Delta_T}\right) - w + I_{syn} \tag{1}$$
$$\tau_w\frac{dw}{dt} = a(V - E_L) - w$$

When the membrane potential crosses a threshold, a spike is emitted, and the

system is reset as in the equation (16).

$$\text{if } V \geq V_D \quad \text{then} \quad \begin{cases} V \rightarrow V_R \\ w \rightarrow w + b \end{cases} \tag{2}$$

Parameters used for the excitatory (RS) and inhibitory (FS) populations are respectively $V_t = -50$ mV and $V_t = -48$ mV, $D_t = 2$ mV and $D_t = 0.5$ mV, $b = 100$ pA and $b = 0$ pA, and $\tau_w = 1000$ ms for RS. For both population: $C_m = 200$ pF, $g_l = 10$ nS, $E_l = -65$ mV, $a = 0$ nS, $V_{reset} = -65$ mV, $t_{refractory} = 5$ ms.

In order to compare some of the results obtained with the AdEx model we used two other models of neuronal activity. First the Conductance-based Adaptive Exponential integrate-and-fire model (CAdEx), which solves some of the limitation of the AdEx model (Górski, Depannemaecker, & Destexhe, 2021). The equation are as follow:

$$\begin{aligned} C\frac{dV}{dt} &= g_L(E_L - V) + g_L\Delta_T \exp\left(\frac{V - V_T}{\Delta_T}\right) + g_A(E_A - V) + I_s \\ \tau_A\frac{dg_A}{dt} &= \frac{\bar{g}_A}{1 + \exp\left(\frac{V_A - V}{\Delta_A}\right)} - g_A \end{aligned} \tag{3}$$

When the membrane potential crosses a threshold, a spike is emitted, and the system is reset as in the equation (16).

$$\text{if } V \geq V_D \quad \text{then} \quad \begin{cases} V \rightarrow V_R \\ g_A \rightarrow g_A + \delta g_A \end{cases} \tag{4}$$

Parameters used for inhibitory (FS) populations are: $g_l = 10$ nS, $E_l = -65$ mV, $V_T = -50$ mV, $ga = 0.$ nS, $E_A = -70$ mV, , $\delta g_A = 0$ nS, $C = 200$ pF,

$\Delta_T = 0.5$ ms, $V_A = -45$ mV, $Is = 0.0$ nA, $refractory = 5$ ms, $V_{reset} = -65$ mV, $tau_A = 0.01$ ms, $\Delta_A = 0.5$ mV and for the excitatory (RS): $g_l = 10$ nS, $E_l = -65$ mV, $V_T = -50$ mV, $\delta g_A = 1$ nS, $E_A = -65$ mV, $\delta g_A = 1$ nS, $C = 200$ pF, $\Delta_T = 2$ mV, $V_A = -30$ mV, $Is = 0.0$ nA, $t_{refractory} = 5$ ms, $V_{reset} = -65$ mV, $tau_A = 1.0$ s, $\Delta_A = 1$ mV

Then we use the Hodgkin-Huxley model (Hodgkin & Huxley, 1952), hereafter denoted HH, with the following equations:

$$C_m \frac{dV}{dt} = -g_l(E_l - V) - g_K n^4 (V - E_K) - g_{Na} m^3 h (V - E_{Na}) + I_{syn} \quad (5)$$

with gating variables (in ms):

$$\frac{dn}{dt} = \frac{0.032(15. - V + V_T)}{(exp(\frac{15. - V + V_T}{5.}) - 1.)}(1. - n) - 0.5exp(\frac{10. - V + V_T}{40.})n \quad (6)$$

$$\frac{dh}{dt} = 0.128exp(\frac{17. - V + V_T}{18.})(1. - h) - \frac{4.}{1 + exp(\frac{40. - V + V_T}{5.})}h \quad (7)$$

$$\frac{dm}{dt} = \frac{0.32(13. - V + V_T)}{(exp(\frac{13. - V + V_T}{4.}) - 1.)}(1 - m) - \frac{0.28(V - V_T - 40.)}{(exp(\frac{V - V_T - 40.}{5.}) - 1.)}m \quad (8)$$

With $C_m = 200$ pF, $E_l = -65$ mV, $E_{Na} = 60$ mV, $E_K = -90$ mV, $g_l = 10$ nS, $g_{Na} = 20$ nS, $g_K = 6$ nS, $V_{Texc} = -50$ mV, $V_{Tinh} = -52$ mV.

For all types of neuron models, the parameters have been chosen in biophysical range (see (Naud et al., 2008; Górski et al., 2021; Hodgkin & Huxley, 1952; Hille, 1992)) in order to keep the basal asynchronous irregular activities (Brunel, 2000) into a range of firing rate coherent with experimental observations (El Boustani, Pospischil, Rudolph-Lilith, & Destexhe, 2007).

The network is built according to a sparse and random (Erdos-Renyi type) architecture where a fixed probability of connection between each neurons is set to 5%. We considered a network model of ten thousand neurons, built according

to specific properties of the cortex. This network is made of an inhibitory (FS) and an excitatory (RS) population, respectively representing 20% and 80% of the total size of the system as previouly done in (Carlu et al., 2020) The communication between neurons occurs through conductance-based synapses. The synaptic current is described by the equation (21).

$$I_{syn} = g_E(E_E - V) + g_I(E_I - V) \tag{9}$$

Where $E_E = 0$ mV is the reversal potential of excitatory synapses and $E_I = -80$ mV is the reversal potential of inhibitory synapses. g_E and g_I, are respectively the excitatory and inhibitory conductances, which increase by quantity $Q_E = 1.5$ nS and $Q_I = 5$ nS for each incoming spike. The increment of conductance is followed by an exponential decrease according to the equation (22).

$$\frac{dg_{E/I}}{dt} = -\frac{g_{E/I}}{\tau_{syn}} \tag{10}$$

with $\tau_{syn} = 5$ ms

The network thus formed receives an external input, based on the activity of a third population (excitatory) of the same size as the excitatory population. Each of its neurons is connected to the rest of the network according to the same rule as mentioned earlier (fixed probability of 5 % for each connection). This external population produces spikes with a Poissonian distribution at a given tunable rate. The external perturbation that mimics the incoming seizure occurs through the augmentation of this firing rate.

The shape of the latter is described by the equation (23).

$$\begin{aligned}\nu_{pert}(t) = \beta + \alpha * (exp(-(t-T_1)^2/(2.*\tau_{on}^2)) * H(-(t-T_1)) \\ +H(-(t-T_2)) * H(t-T_1) + exp(-(t-T_2)^2/(2.*\tau_{off}^2)) * H(t-T_2))\end{aligned} \tag{11}$$

where H is the heaviside function and $\beta = 6$ Hz is the basal constant input. This function takes the general form of a high plateau, where T_1 and T_2 are the times when the perturbation reach its beginning and end respectively, and α defines its maximal height. τ_{on} and τ_{off} are respectively time constants associated with the exponential rise and decay of the perturbation.

2.2 Coarse graining and continuous analysis

In order to analyse in details what mechanisms are at play in the network during a seizure-like event, we resort to a combination of two methods : a so-called *structural coarse-graining*, that is we gather neuron models in n groups according to their inhibitory in-degree (the number of inhibitory connections they receive, we justify this approach in the body), and we study their time evolution through statistics of their membrane potential (mean and alignment) over these groups. In other words, at each integration time step, we will obtain n values of mean membrane potentials, one for each group, as well as n values of Kuramoto order parameter (measuring alignment in groups).

To obtain the Kuramoto order parameter, we first transform the single neurons membrane potentials into phase variables by applying a linear mapping $v_j \in [V_R, V_D] \rightarrow \theta_j^v[0, \pi]$. Then the Kuramoto order parameter is computed through the equation (24).

$$R \exp i\Psi = \frac{1}{N} \sum_j \exp i\theta_j^v \tag{12}$$

$R \in [0, 1]$ gives the degree of "alignment" (if it persists in time, one would say synchronization) : $R = 1$ implies full alignment , while $R = 0$ implies no alignment whatsoever. $\Psi \in [0, \pi]$ tells us the mean phase of the transformed variables (directly related to the mean membrane potential).

Let us mention one caveat here. The membrane potentials are not mapped on the full circle, to avoid artificial periodicity of the obtained angles: having $V = V_R$ is not the same as having $V = V_D$. One may thus ask why such a measure is used instead of the usual measures of dispersion such as the standard deviation. We use the Kuramoto order parameter because it gives a naturally normalized quantity, thus allowing a direct comparison of what is happening at each time step. We acknowledge that it would be formally possible to use a normalized version of standard deviation, but the normalization procedure involved would not be as intuitive. Besides, the Kuramoto order parameter allows direct calculation of higher order types of alignment by using the generalized version: adding an n multiplier to the exponential would give a measure of the degree of partitioning into n clusters, which can turn out to be useful in subsequent studies.

2.3 Code Accessibility

The code/software described in the paper is freely available online at [URL redacted for double-blind review]. The code is available as Extended Data and is run on Linux operating system.

3 Results

In this section we show how, in networks of various neuron models, a paroxysmal external stimulation can trigger a crisis or not, depending on various parameters. We show how the situations differ from model to model and what

are the common features. Then, we turn ourselves to a structural analysis based on mean firing rates of individual neuron models to guide a particular coarse-graining, which we use as a filter to observe the dynamics and gain further understanding, from both qualitative and quantitative perspectives. Finally we show how this study can guide proactive approach to reduce the chances of crisis propagation.

3.1 Propagative and Non-propagative behaviors

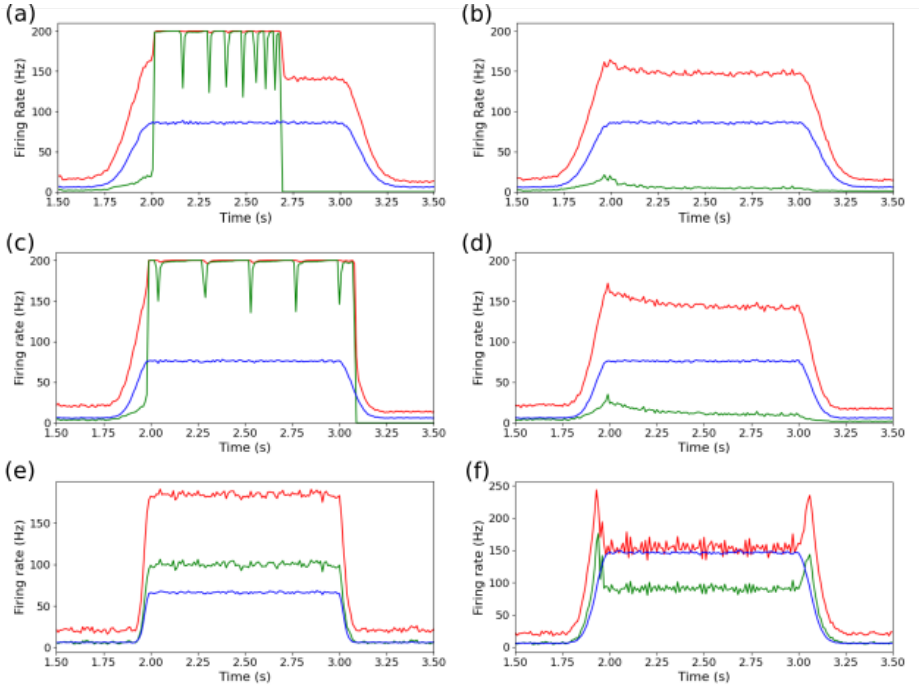

Figure 2: **Firing rate of the network populations in response to a perturbation**: propagative and non-propagative behaviors (respectively left and right columns) for AdEx model ((a) and (b)), with amplitude of perturbation $\alpha = 80Hz$ and $\tau_{slope} = 100ms$; CAdEx model ((c) and (d)) with $\alpha = 70Hz$ and $\tau_{slope} = 80ms$; HH model (e) with $\alpha = 60Hz$ and $\tau_{slope} = 60ms$ and (f) with $\alpha = 140Hz$ and $\tau_{slope} = 60ms$. [FIGURE MODIFIED]

In this study we assume that the networks depicted in the previous section

represent a small cortical area receiving connections from an epileptic focus. Specifically, the arrival of the seizure is modeled by a sudden rise in the firing rate of the external (afferent) Poisson region where the crisis comes from, or originates. In other words, we are not concerned with how crises *originate* (epileptogenesis), but how they can *propagate*. Therefore, we will frame our analysis into two main behaviors : *propagative*, *i.e* the network develops an excitatory firing rate greater than the input, which makes it able to propagate the crisis to efferent regions, and *non-propagative* behavior where the excitatory firing rate is lower than the input, thus attenuating the incoming signal.

As mentioned (and detailed) in the method section, the perturbation starts with an exponential growth followed by a plateau and ends with an exponential decrease, going back to the basal level, see blue curves in Fig.2). We show in this figure the response of the various networks to this type of disturbance. Here we can distinguish between two classes of macroscopic differences between propagative and non-propagative scenarios : one where the difference is binary (AdEx and CAdEx), *ie* the network either features

a very strong increase in the firing rate of the inhibitory *and* excitatory populations, either the sharp increase in the firing rate concerns the inhibitory population only, thus strongly limiting the activity of the excitatory population (consequently preventing the disturbance from spreading to the next region). From this perspective, the propagative scenario can be understood as a loss of balance between excitatory and inhibitory firing rates, which the network struggles to find once the excitatory population has exploded. Interestingly these two scenarios can occur for the same global shape of the perturbation but changing only the noise and network realizations. It must be noted that the $200Hz$ maximum frequencies measured here are the results of the temporal binning of the global spiking dynamics, taken as $T = 5ms$, which corresponds to

the refractory time of the single neurons in Adex and CAdEx. Upon choosing a shorter binning, *e.g* $T = 1ms$, higher frequency peaks are observed, going up to $800Hz$, thus hinting at overall faster dynamics. The second class (HH) shows a rather continuous difference between propagative and non-propagative behaviors, depending on the amplitude of the perturbation (this will become clearer in the next section). This said, there is still some degree of stiffness in the HH scenario, where the non-propagative case shows peaks of both excitatory and inhibitory activities at the beginning and end of the plateau.

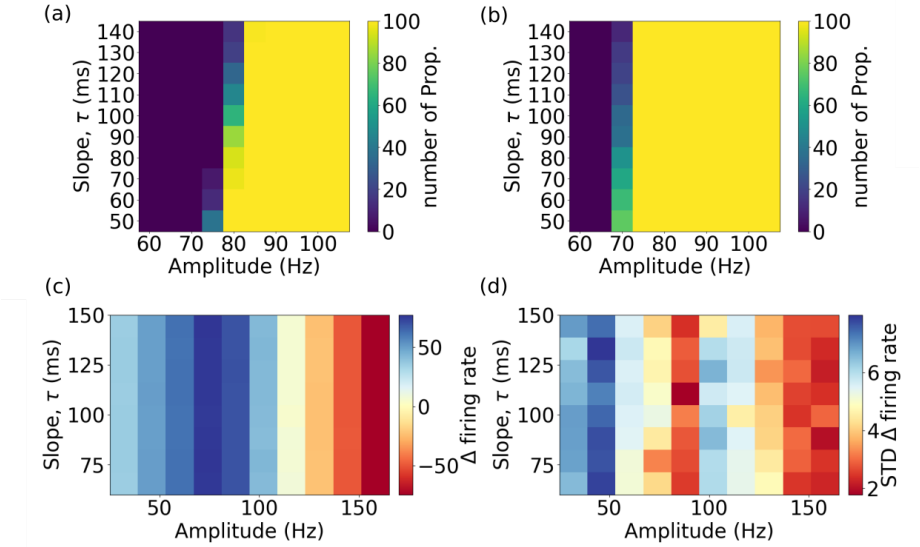

Figure 3: **Grid search on the amplitude and slope of the incoming perturbation for each network.** Panels (a) and (b) show the number of realizations which propagate, respectively for Adex and CAdEx networks. Panels (c) and (d) show respectively, for HH networks, the means and standard deviations (over realizations) of the difference of firing rates between excitatory and Poisson populations ($\Delta\ firing\ rate = \nu_e - \nu_{Pois}$), averaged over the length of the plateau.[FIGURE MODIFIED]

3.2 Parameter search

To study how the shape of the perturbation affects the networks response, we screened different time constants of the exponential growth rates and maximum amplitude of the plateau with 100 seeds (for both network and noise realizations) for each couple of values, see Fig.3)

and probed, in the case of AdEx and CAdEx (respectively (a) and (b), the number of realizations which *did not* yield propagative behavior. In the HH case, the perspective is a little different : we chose to show two figures, displaying means and standard deviations over realizations of the difference in firing rate between excitatory and Poisson populations (averaged over the plateau), $\Delta\ firing\ rate = \nu_e - \nu_{Pois}$ rate (respectively (c) and (d)). As can be expected, for all networks (AdEx, CAdEx and HH) the amplitude of the perturbation plays a determinant role in the type of scenario we eventually find (propagative or not), however in opposite directions and of different nature. Indeed, for both AdEx and CAdEx, increasing the amplitude increases the chance of having a propagative scenario for a fixed slope, in a binary fashion, while in the case of HH the contrary is observed, and in a continuous fashion. Furthermore, in AdEx and CAdEx networks, we observe that when the arrival of the disturbance is abrupt (i.e. small time constant for exponential growth), it is systematically propagative, no matter which amplitude is considered in the range $[60 - 120Hz]$. On the other hand, if the perturbation rises sufficiently slowly (i.e. large exponential time constant), it does not significantly affect the excitatory population of the network. These observations show that we are dealing with a phenomenon where dynamics play a crucial role. Also, we observe a slight coupling effect between slope and amplitude : for higher amplitudes, the propagation range extends to slower perturbations. On the contrary, in the HH network, it seems that the slope does not play any major role, hinting

at a much less dynamical effect : the difference manifest themselves as local equilibria of the networks under considerations, reached no matter the time course. Moreover, the standard deviations, besides showing no clear dependence on neither amplitude nor slope, are very small compared to the means, thus evidencing that noise neither plays any significant part here. These observations highlight once again deep differences between the two types of network and their respective phenomenology.

Interestingly, in the case of AdEx and CAdEx, there exists a limit, bi-stable region where the perturbation may or may not propagate in the network, depending on the noise realisation. Thus, the global scenario does not trivially depend on the amplitude and time constants of the perturbation in this region, which, besides being of primary importance in the case of seizure propagation, also makes it a perfect candidate to study more deeply the internal mechanisms at play, and will thus be the main focus of the remainder of this paper.

3.3 Influence of structural aspects on the dynamics

In the following, we turn our attention to the bi-stable region of AdEx and CAdEx networks, where the two behaviors are present, and investigate what can be the source of the divergence. There are two main differences between the simulations under consideration: the realization of the network structure and the realization of the external input, as both rely on random number generators. We have therefore successively fixed each of them, and observed that the two behaviors were still present. Also, the global scenarios were indistinguishable from those showed so far. First, this allows us to fix the network structure (which will become determinant in this part) without losing the richness of the phenomenology. Second, this tells us that what shapes the distinction between the two phenomena is more complex than a single question of structure, or real-

ization of the input. Another perspective is then needed to explore the internal dynamics of the network in both scenarios. As the models into consideration have very large number of dimensions, as well as quite intricate structures, brute force analytical approaches are simply not conceivable.

Let us then take a step back and investigate the relationship between the firing rate of each neuron and its number of afferent (input) connections of the three kinds: excitatory (N_{inp}^{Exc}), inhibitory (N_{inp}^{Inh}) and Poissonian (N_{inp}^{Pois}). Fig.4(a) shows the average firing rates (ν_E^{NP} and ν_I^{NP}) measured over the whole non-propagative (NP) scenario for each neuron in the AdEx network (simply defined as the total number of spikes divided by the total integration time, after having discarded a transient), plotted as a function of the three different connectivity profiles.

Note here that averaging over simulations for the sake of robustness might be a delicate matter, as we might lose constitutive differences in the process. As we are dealing with highly variable situations, we have to make compromises between generalizability and relevance. Therefore, we start with a single realization to then guide larger and more systematic investigations.

Interestingly, we see a much stronger influence coming from the inhibitory in-degree than from the Poissonian and excitatory ones. Counter-intuitively, it even seems that excitatory in-degree has barely any effect at all on total measured firing rates. Indeed, from the point of view of Pearson's correlation, inhibitory in-degree is much more (anti)-correlated with the firing rate than the excitatory in-degree (almost no correlation) or the Poissonian in-degree (little correlation). Note that we observe the same structure for propagative situations (results not shown). This said we can compile the previous results and analyze whether the most salient in-degrees (inhibitory and Poissonian) has any influence on the *difference* between propagative and non-propagative situations, see

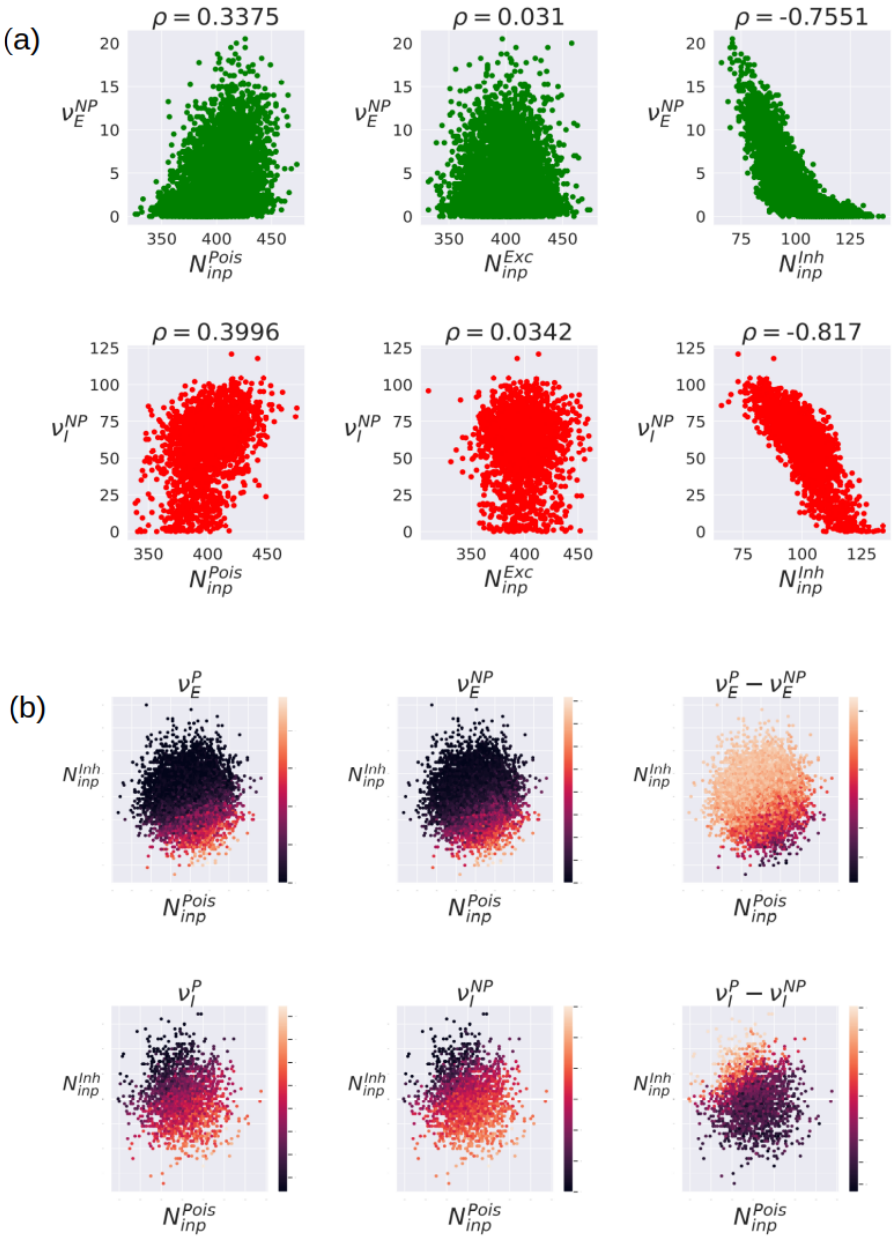

Figure 4: **Influence of connectivity on single neurons firing rates:** (a) Influence of poissonian (N_{inp}^{Pois}), excitatory (N_{inp}^{Exc}) and inhibitory (N_{inp}^{Inh}) input connectivity on the firing rates of excitatory neurons (ν_E^{NP}), and inhibitory ones (ν_I^{NP}) in non-propagative scenario (NP) of the AdEx network. The standard pearson correlation coefficient ρ is estimated. (b) Time averaged single neuron firing rates and differences in propagative vs non-propagative regimes, as a function of both inhibitory and poissonian in-degrees.[FIGURE MODIFIED]

Fig.4(b).

Here we see that the global dependency of the average single neuron firing rates on inhibitory and Poissonian connectivity does not qualitatively change between propagative and non-propagative regimes. However, the difference displays an inverse dependency on both variables: despite maintaining the same general hierarchical structure, the crisis tends to compensate a little bit for it. In other words, the neurons that are initially less firing, due to their structural properties, are the most impacted by the crisis. Furthermore, it must be noted that, although there is no correlation between inhibitory and Poissonian in-degrees (as can be expected from random connectivities), we still see a slope of the firing rate in the 2D+color representation, highlighting that they both play a role in the single neurons long term dynamics.

Although these results are not sufficient to explain the propagation or non-propagation behaviors, it is already worth pointing that, not only they establish a first link between structure and dynamics, but give insight on how *differences* of dynamics are correlated with structure, hence giving interesting leads on possible ways of analyzing time-series. Indeed one can think of deploying algorithms to infer structural or functional connectivity from the spiking regimes of single neurons in both "nominal" and crisis dynamics, as well as their difference.

However, it seems necessary from our current perspective to go deeper into the temporal evolution. In order to probe whether the differences in the individual mean firing rates give single neurons specific roles in the dynamics, we now start classifying in the AdEx network the indices of the neurons in the raster plot according to the total number of spikes they emit during the whole simulation. We chose for this purpose a representative propagative scenario for two reasons : 1) it is clearly the most consequential case in the context of seizure dynamics and spreading, hence 2) if no distinction is visible here, the previous

static approach (in the sense "time-averaged") would be of little dynamical relevance. The sequence of propagation of the perturbation then appears visually, see Fig.5(a). We observe, in the case of propagation a fast cascade, which is consistent with the experimental observations (Neumann et al., 2017): the model shows that some neurons are quickly "entrained" in a sequence at the onset of the seizure. In addition, there is no perfect synchronization of the action potentials of all neurons. This is an interesting result, coherent with the observations on epilepsy in the last decade (Jiruska et al., 2013).

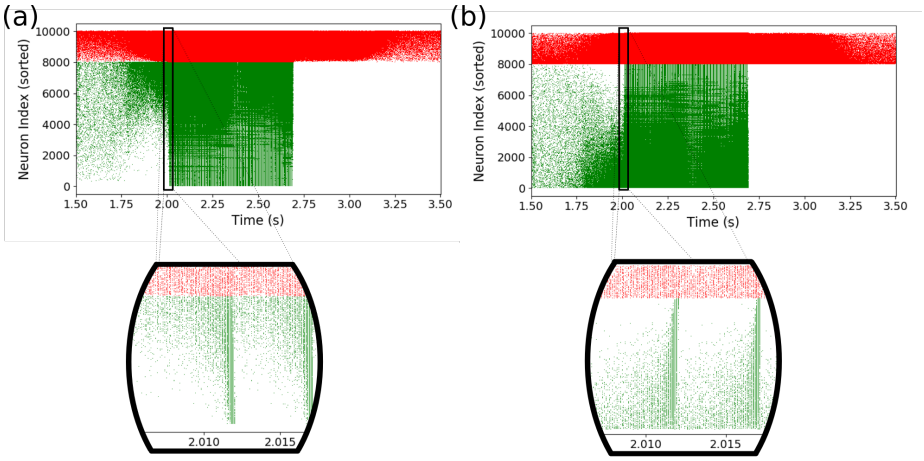

Figure 5: **Dynamics in propagative situation (AdEx):** (a) Raster plot of a simulation with propagative behavior, neuron indices are sorted according to the number of spikes during the simulation. A "cascade" phenomenon can be observed when zooming on the onset of the perturbation propagation in the excitatory population. (b) The same cascade phenomenon is observed when neuron indices are sorted in function of the number of inhibitory inputs received.

Secondly, we examine the same situation, but sorting neuron indices as a function of the number of inhibitory inputs they receive (as shown Fig. 5(b), as it is the most influential structural feature we observed. Here too, the cascade phenomenon is clearly visible, showing that the inhibitory input connectivity has a central influence on the dynamics at play during the perturbation.

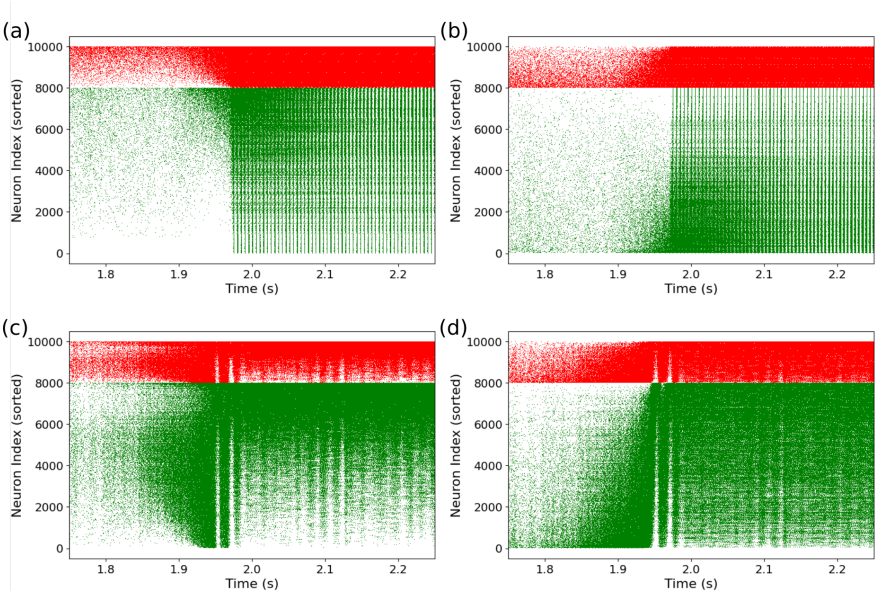

Figure 6: **Dynamics in propagative situation (CAdEx and HH):** Same plot as previously shown but for CAdEx network ((a) spike-sorting, (b) inhibitory in-degree sorting) and HH network ((c) spike-sorting, (d) inhibitory in-degree sorting). Cascade phenomena are still observable in panels (a),(b) and (d), hence showing its robustness, but not in (c), where propagation takes a slightly different form, highlighting the contrast induced by different perspectives on a single complex dynamics.[NEW FIGURE]

Fig.6 shows the same pictures for CAdEx and HH networks. We see here that CAdEx network's behaviors are very similar to AdEx : sorting with firing rate or inhibitory in-degree give very similar structures and we can distinguish here too the cascading effect at the onset of the perturbation, following the indices. HH networks show quite a different phenomenology. First the two sorting do not show the same structures, which hints at a more sublte mapping between inhibitory in-degree and long-term single neuron model dynamics. In the firing rate sorting, we can still distinguish 3 blocs of distinct activity, and thus of populations, corresponding to the 3 key periods of the simulation : before stimulation, at the onset, and during the stimulation. Interestingly it seems that before and during the stimulation different populations of neuron models are

distinctly mobilized. While before the stimulation, the central neurons (with respect to their indices) are active, a double cascade contaminates the rest of them (towards higher and lower indices) at the onset, ending in a general surge of activity. This must be contrasted with the in-degree sorting panel, where the cascade is more unidirectional, as the main activity slides from low connectivity indices (less connected) to the higher ones, until all neurons fire. This emphasizes the importance of the perspective chosen to analyse complex behavior.

Altogether these results show the relevance of adopting a perspective based on the inhibitory in-degree : it yields interesting insights on the internal organisation of the network before and during the paroxysmal event. In the next section, we push further this analysis by comparing propagative and non-propagative scenario, and make use of the continuous measures introduced in Material and Methods.

3.4 Continuous measures on subgroups of neurons

We now move to a deeper investigation of the AdEx networks behavior, in order to better grasp the internal dynamical structure into play. We chose this model among the three because : 1) it is the simplest, which 2) reduces the computational burden for a more systematic analysis, although 3) it can still yield various types of single neuron dynamics (which makes it a relevant model per se) and 4) is widely use for neuronal network simulations. To achieve so, we first consider groups of neurons defined by their inhibitory in-degree. These are somewhat artificial, as they are only statistical reflections of topological aspects of the network (i.e, there is no reason to think a priori that all neurons having n inhibitory inputs would have more privileged links among themselves than with those having $n + 1$). However, they allow in principle a variable degree

of categorization, based upon the sampling of the inhibitory in-degree distribution, which eventually leads to different levels of (nonlinear) coarse-graining (although we will consider only one such sampling here). This is a first bottom-up step towards a coarser description of the system, and hence, may guide reliable modeling attempts at larger scales. Secondly, we switch our analysis to continuous variables, which allow a finer and more systematic analysis of the dynamics, as they don't depend on spike times. Indeed, although spike timings are the most accessible collective measures in real-life systems, which make them the most fitted candidates for "transferable" studies, we want here to take advantage of the virtues of mathematical modeling to probe the insides of these simulations, to then be able to draw conclusions on more accessible observables. We focus here uniquely on membrane potentials, as they are the closest proxy of the firing dynamics in the network and chose to use two main measures based on them: the mean μ_V and a modified Kuramoto order parameter R, which gives a naturally normalized measure of instantaneous alignment (or similarity) of the membrane potentials. Both are defined in time, over a class of neurons. Note here that the network connectivity *is still* held fixed, as these calculations require a lot of time and computational power, especially as we always consider 50 noise realizations. We will give evidence of the robustness of our observations in the next part.

Mean membrane potential in time

We show in Fig.7(a)-(b) the mean membrane potential μ_V defined for each group of excitatory (RS) and inhibitory (FS) neurons in time, averaged over realizations (top row), and standard deviation over realizations (bottom row), in propagation (a) and non-propagation (b) scenarios. The different realizations refer here to the incoming noisy input, while the network structure is held fixed.

All the data presented from now are obtained by regrouping neurons having the exact same inhibitory in-degree, thus corresponding to a discrete one-to-one sampling of the input distribution. Note that, given the network architecture under consideration, the mean number of afferent inhibitory synapses, defined over both populations of neurons, is defined by $\mu_i = N_i \times p_{connect} = 2000 \times 0.05 = 100$, where N_i is the total number of inhibitory neurons and $p_{connect}$ is the connection probability, while the standard deviation is $\sigma_i = \sqrt{N_i \times p_{connect}} = 10$. Besides, the groups are defined operationally, by grouping in the range $n \in [0, 200]$ the neurons receiving n inputs. Thus, if no neuron receives n inputs, the group is not represented. Accordingly, having approximately 60 groups tells us that we sample the distribution from around ± 30, that is $3\sigma_i$.

We see from this figure that the inhibitory in-degree profile seems to play a major role in the overall dynamics. Indeed, as the perturbation is growing, we can first observe a strong effect on the mean membrane potential of every excitatory neuron, then followed by a low-potential cascade initiated from weakly coupled neurons and following the group structure. This latter effect is much clearer in the case of inhibitory neurons, where the cascade follows very well the input profile, in both propagative and non-propagative scenarios. Note that the low-potential area can be easily understood as a high-firing regime: neurons fire as soon as they leave their resting potential, thus displaying very low values of membrane potential when calculated (and sampled) over time.

Interestingly these pictures show that, up to the decisive point of the crises, the continuous measures look very similar, thus hinting at an instantaneous finite-size fluctuation causing the whole network to explode. Also, it is noteworthy that the new "hierarchy" set by the cascade is conserved in the non-propagative regime, while propagation seems to have an overall reset effect.

Also, we see from these graphs that there is a particular time window where

the variance of the mean membrane potential is larger for the most inhibitory-connected neurons, in both RS and FS populations (although it appears clearer for RS ones here, because of the need to rescale the FS colorbar to have comparable results). We found that this time window defines the period when the network can actually switch to propagation: the high variance corresponds to different times when various realizations "explode", and thus defines a region of instability.

A central point to raise here is that what makes the difference between propagative and non-propagative scenarios is most likely *not* an *infinitesimal* instability defined from a macroscopic perspective, i.e, that is due to a positive eigenvalue of a Jacobian defined from a large scale representation (Mean-Field for example), otherwise the non-propagative behavior would simply not be observable (as, except for chaotic dynamics, we do not observe unstable trajectories in phase space). Indeed, what differs between the various simulations is the noise realization of the external input, which may, or may not, bring the system to a point of instability. The external Poissonian drive, with *finite-size* fluctuations is thus constitutive of the scenarios we observe.

To gain more insight into the diversity of dynamics across neuron groups, we turn our attention to a measure of alignment, or synchronisation, namely the Kuramoto order parameter R.

Kuramoto order parameter

We show in Fig.8(a)-(b) the Kuramoto order parameter R defined for each group of excitatory (RS) and inhibitory (FS) neurons in time, averaged over realizations (top row), and standard deviation over realizations (bottom row), in propagation (a) and non-propagation (b) scenarios.

The cascade previously observed is clearly visible for the average R, in the form of a "desynchronization cascade". We note here that this illustrates a

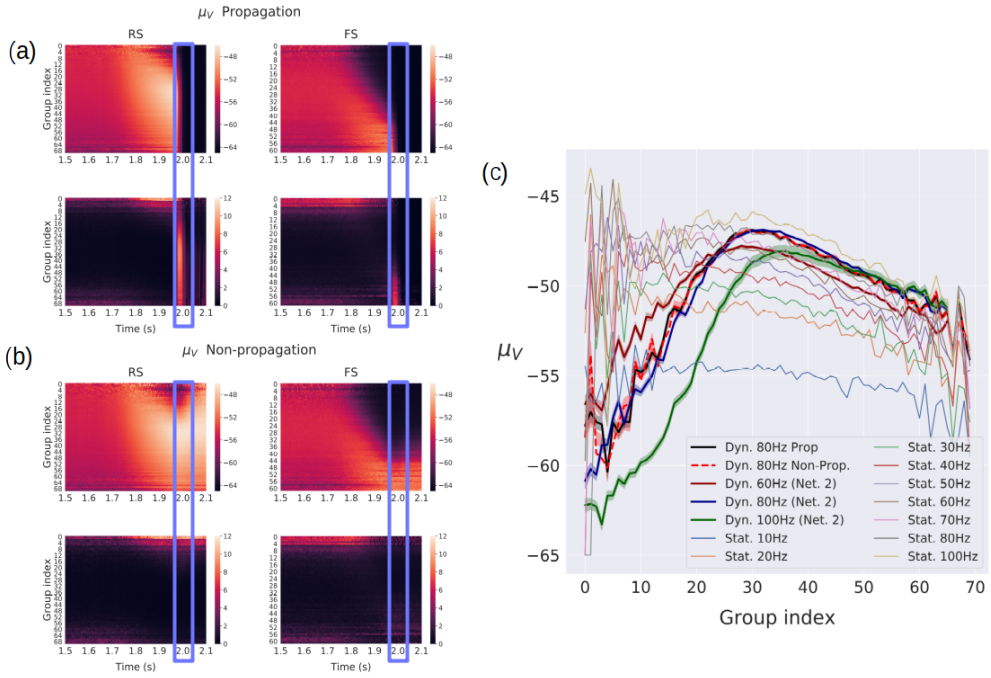

Figure 7: **Mean membrane potential over subgroups of neurons** for each group defined as a function of their incoming inhibitory connections, averaged over 50 noise realizations (17 non-propagative and 33 propagative). Color maps correspond for each group to the average membrane potential (top) and standard-deviation (bottom) across noise realizations in the propagative situations (a) and non-propagative situations (b) for both excitatory (RS) and inhibitory (FS) populations. The blue windows highlight the (time) region where the system either switches to a propagative regime, or remains stable. (c) Steady-state profiles (for fixed external input) of μ_V for RS neurons, together with various profiles for different amplitudes of perturbation, captured right before typical time of crisis, at respectively 1950ms (60Hz), 1950ms (80Hz), 1930ms (100Hz, as the crisis develops *before* 1950ms). Networks are the same as previously analyzed, except when stated Net. 2. Standard errors estimated over noise realizations are shown in shaded areas.[FIGURE MODIFIED]

recruitment process between two radically different regimes having nonetheless similar alignment features : a fluctuation-driven asynchronous irregular (AI) dynamics, where membrane potentials are mostly conditioned by the balance of inhibitory versus excitatory inputs, and a crisis characterized by high spiking and membrane potentials clamped by refractoriness. The desynchronization cascade thus establishes a strict limit between them, while showing a significant degree of symmetry : the times right before or right after the cascade are indistinguishable, from the point of view of the inhibitory neurons, except at the end of the non-propagative regime. Interestingly in this case, it appears that the misalignment of the neuron groups finally attained is constantly fueled by the network, thus hinting at a fundamentally out-of-equilibrium steady state. From the standard deviation perspective, two main features are worth pointing. First, we can again clearly observe the instability window, characterized by high standard deviation between realizations in propagative scenarios. Secondly, we can observe a significant variability between the various cascades observed in excitatory cells (particularly the low indices), while a very weak one for inhibitory ones. In other words, the excitatory cascade may take various forms in both propagative and non-propagative scenarios, while the inhibitory one remains quite robust, even with respect to the non-equilibrium state mentioned before.

3.5 Dynamic versus static approach

We have seen that changing the slope and the amplitude of the signal may trigger (or not) a crisis, thus hinting that the time evolution of the perturbation is central. Then we observed a hierarchical structure setting in from the point of view of continuous measures, following the perturbation. However, fundamental questions remain: how much of this latter phenomenon is actually dynamic? Would we find the same structures if we bombarded the network with a fixed

input at, say, $80Hz$? Can we observe the same structures for scenarios which are always, or never, propagative (no matter the noise realization) ? This would indicate that the structures observed thus far might have little to do with the crisis phenomenology itself but would either be the mere results of strong conditioning of the network by the level of input (if static structures are similar), or simply not yield any explanation for the instability we observe (if always/never propagative scenarios show similar features).

We now turn our attention to Fig.7(c), which displays the static μ_V profiles in RS population obtained for fixed external inputs (Stat. curves), together with the profiles captured at the typical onset of the crisis, for various amplitudes: 60Hz (never propagative), 80Hz (sometimes propagative) and 100Hz (always propagative). The network realization is the same as previously analyzed, except when explicitly stated (Net. 2), where we refer to another connectivity. For the 80Hz scenarios with the first network (the one we have been investigating so far), we kept the splitting of the realizations between propagative and non-propagative, to highlight the potential differences of structures.

First, as previously observed, the profiles obtained for propagative versus non-propagative regimes are very similar at the onset. Then, we clearly see that the μ_V profiles extracted from the dynamical situations (hereafter called the dynamical profiles) are very different from the static ones.

Besides, it is worth pointing that the profile obtained for a 80Hz amplitude with a different random realization of the network (where all 50 noise realizations are put together, based on the previous observation that propagative and non-propagative scenarios show very similar structures) is very similar to those already shown, with small standard error, which, together with the previous observation that noise and network realizations seem to play similar roles, underlie a robust network phenomenology. Furthermore, we see that the profiles

obtained for 60Hz, 80Hz and 100Hz amplitudes *are different*. The nature of their differences is of great interest for low indices, where we observe that 60Hz and 100Hz profiles are located on opposite sides of the central 80Hz profile: their ordering in this region is consistent with that of their degree of instability we have observed so far. This said, the dynamical profiles yet show similar qualitative features : they all are non-monotonous and display two well-separated parts. Indeed, for low indices (until 30) μ_V is increasing with values starting around the lowest of the static profiles (10Hz), while their high indices part is more aligned with high static profiles. Interestingly, we see that for 60Hz and 80Hz the right part is well aligned with the static profile obtained for similar inputs. This does not seem to be the case for 100Hz, although the static input simulation displays some instability, which makes their comparison less relevant. Although it is not straightforward to link μ_V with the instantaneous regime, we have seen that low values can be associated with high firings (the neurons spending most of their time clamped at -65mV). This would help understanding what is happening here: for higher values of amplitude, the less inhibitory-connected neurons are firing more, and can thus entrain the rest of the network.

Fig.8(c) shows the Kuramoto counterpart of the latter figure. Here the R profiles display structures quite different from those observed for μ_V. Indeed, the various static profiles do not display such clear variability as for μ_V, although little differences can still be observed: high inputs seem to show more variability in low indices, while ending at higher values for higher indices. More importantly, the dynamical profiles are here too very different, from the static ones, and among themselves. Besides, propagative and non-propagative simulations show little differences here too, and the profiles corresponding to same amplitude (80Hz) and different network architecture (Net. 2) also overlap here.

Interestingly we can also observe that the 60Hz and 100Hz profiles are different and located apart from the 80Hz, although they also show different magnitudes of their inverted peaks. Given that the ordering of these magnitudes are not consistent with the various degrees of instability, we suggest that the *position* of the peak might be the relevant criterion. This would be consistent with the observations we made thus far, and confirm our previously suggested scenario: as the more we approach the center group, the more neurons are considered (gaussian distribution), the green peak (100Hz) tells us that more neurons have undergone the desynchronization cascade we mentioned earlier, that is, more neurons have already "switched side" and entered a high firing regime, thus giving more inertia to the cascade phenomenon. The middle scenario (80Hz) would then sit on a *tipping point*, that is a point separating two radically different dynamical regimes of the system.

These latter observations show that, from the perspective of both mean membrane potential and Kuramoto order parameter calculated inside the groups formed from inhibitory in-degree, we are in the presence of a structured behavior which emerges from an intricate interaction between dynamics and architecture, and which cannot be recovered from static approaches. Moreover, the various sizes of the groups and their impact on the phenomena we observe highlight that multiscale dynamics is a hallmark of the observed scenarios.

3.6 Can seizure propagation be controlled by external inputs?

Now that we have established how the structure of the dynamics allows or not the propagation of the paroxysmal perturbation (although the proximal cause relies on noise fluctuations), we investigate whether we could use the previous finding of a strong instability window for the 80Hz dynamical scenario to

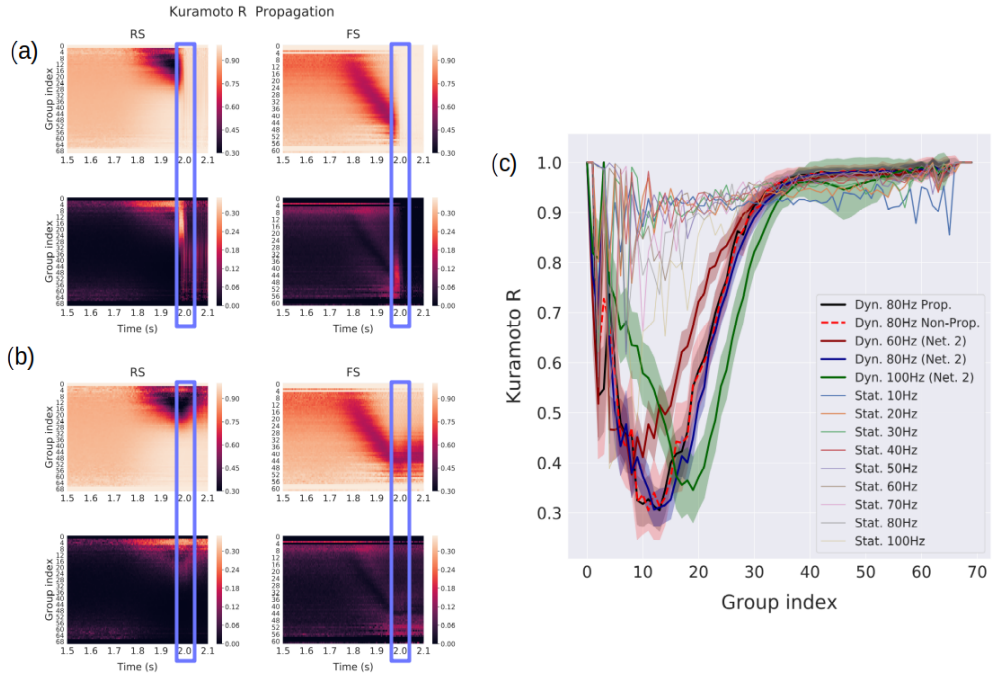

Figure 8: **Kuramoto R of membrane potentials over subgroups of neurons** for each group defined as a function of their incoming inhibitory connections, averaged over 50 noise realizations (17 non-propagative and 33 propagative). Color maps correspond for each group to the average membrane potential (top) and standard-deviation (bottom) across noise realizations in the propagative situations (a) and non-propagative situations (b) for both excitatory (RS) and inhibitory (FS) populations. The blue windows highlight the (time) region where the system either switches to a propagative regime, or remains stable. (c) Steady-state profiles (for fixed external input) of R for RS neurons, together with various profiles for different amplitudes of perturbation, captured right before typical time of crisis, at respectively 1950ms (60Hz), 1950ms (80Hz), 1930ms (100Hz, as the crises develops *before* 1950ms). Networks are the same as previously analyzed, except when stated Net. 2. Standard errors estimated over noise realizations are shown in shaded areas.[FIGURE MODIFIED]

alter the fate of the AdEx network dynamics. This approach is based on the following reasoning : we have observed, with a detailed analysis, the existence of a particular time window in the network under consideration (Net. 1) in this scenario, which implies a strong uncertainty on its global response. Thus, we want to design a stimulation protocol to reduce the chance of crisis propagation, based on this observation, *but which does not require the same level of analysis*, hence making it applicable inline and without the need of extensive computational power.

To achieve so, we apply a Gaussian stimulation, with 10 ms time constant, two different amplitudes (1Hz and 5Hz), positive or negative, *through a variation* of the external excitatory input. For simulations performed under the same conditions, the stimulations were applied at different times as detailed in Tables 1(a)-(b). These tables show, for a total number of 100 simulations (with same network structure but different noise realizations), among which 72 were propagative, what relative percentage of simulations has undergone a triggering and a cancellation of crisis respectively.

We see that it is possible to somewhat "reverse" the situation, thanks to (or because of) the stimulation: in certain cases, it triggers a crisis propagation when none was initially occurring (Table 1(a)), and in other cases, it prevents one (Table 1(b)). We observe that if the possibility of "triggering" the propagation by stimulation can take place for different times of peak, it remains more important when it occurs in the time window identified previously. This effect is even more visible in the reverse situation, in which propagation is prevented. A notably interesting case is that more than 50% of the crises are prevented if a stimulation of -5 Hz is applied in the same time window. This could open interesting leads in furthering qualitative comparisons between computational simulations and real-life situations, and eventually guide future interventions.

(a)

time of peak	+1Hz	+5Hz	-1Hz	-5Hz
t = 1500ms	0.25	0.1786	0.2857	0.25
t = 1850ms	0.178	0.1786	0.2143	0.2143
t = 1950ms	0.0357	0.6071	0.2143	0.5
t = 1975ms	0.7143	1.0	0.25	0.28572
t = 2000ms	0.6071	1.0	0.0	0.0714
t = 2500ms	0.0	0.0	0.0	0.0

(b)

time of peak	+1Hz	+5Hz	-1Hz	-5Hz
t = 1500ms	0.1806	0.1944	0.1528	0.1389
t = 1850ms	0.1389	0.1944	0.0972	0.1528
t = 1950ms	0.1528	0.2361	0.125	0.0694
t = 1975ms	0.0972	0.0	0.3472	0.3889
t = 2000ms	0.0139	0.0	0.25	0.5556
t = 2500ms	0.0	0.0	0.0	0.0972

Table 1: **Triggered and prevented events:** (a) Percentage of triggered propagation events, from an initial number of 38 non-propagative behaviors. Highlight in blue $\geq 25\%$ and in red $\geq 50\%$. (b) Percentage of prevented events, from 72 initially propagative behaviors. Highlighted in blue $\geq 25\%$ and in red $\geq 50\%$. The time of peak corresponds to the moment where the maximum of the stimulus is reached, the amplitude corresponds to a variation of the external input (see the main text)

4 Discussion

In this computational work we studied the response of various spiking neural networks to paroxysmal inputs. We observed that the same networks can display various types of responses, depending on its nature (the neuron model used at its nodes), the shape of the perturbation (here we analysed particularly a plateau-like input with various slopes and amplitudes) and the realization of the random number generator. In the case of AdEx and CAdEx, two radically different responses to a qualitatively similar incoming excitatory perturbation are observed. Indeed, the latter could either contaminate the excitatory population and thus allow the crisis to propagate to efferent areas, or be "controlled" by the activity of the inhibitory population, keeping the excitatory population at a low activity level, thus preventing further propagation. The response of the

network depends not only on the amplitude of the perturbation but also on the "speed" at which it occurs. This is consistent with experimental observations. Interestingly, in the case of a HH network, our investigations show very different network responses, where only the amplitude of the perturbation plays a role and where no variability on noise realizations is observed.

A rich literature shows that seizures can be classified according to their onset/offset features described by bifurcation types(Saggio et al., 2020; Saggio, Spiegler, Bernard, & Jirsa, 2017; Jirsa, Stacey, Quilichini, Ivanov, & Bernard, 2014). The most observed bifurcation at the onset of a seizure is a saddle-node bifurcation (Saggio et al., 2017), which is characterized by an abrupt change in the baseline of the electrophysiological signal (Jirsa et al., 2014). We observed in the current work that perturbations are always propagative in AdEx and CAdEx networks when they rise abruptly in the network. There is here an interesting correspondence revealing the importance of the onset of seizure dynamics, as it has been shown from a clinical point of view (Lagarde et al., 2018). It is worth noting that the absence of such phenomenology in HH networks (for the scenarios we considered) raises interesting questions in the modeling of seizure dynamics, but also more generally in neuronal networks : how the quantitative differences (number of variables) and qualitative differences (types of processes taken into account) in the single neuron models affect the global dynamics ? Are more precise models always the best in all respects ? This places back the importance of the the choice (of model, of parameters) in the center of the discussion : by modeling a neuronal network and observing a phenomenon which resembles reality, *we are not* testing whether the specific ingredients we chose are *constitutive* of this phenomenon, but *how they would be* if they were chosen *a priori*. It is only the systematic *cross-model observations and comparisons*, that can yield such answer as necessary and sufficient ingredients to observe a

phenomenon.

Note that, in clinical observations, the most accessible measurements are made on a macroscopic scale. In the study proposed here, we observe the activities at a smaller descriptive scale by building a network of neuron models. We thus have a complex system of very high dimension, rendering a priori impossible to obtain a simple description of the dynamics, which motivates the statistical approach proposed here. With this type of analysis, we were able to track in time key features of the underlying dynamics, especially those supported by the structure of the network : inhibitory in-degree can be mobilized to *explain* global differences in network response. Indeed, we proposed a coarse-grained description of the network dynamics based on inhibitory in-degree, allowing us to capture internal processes that were not visible at first, and which play a significant role in the global out-of-equilibrium dynamics. This opens the way to a flexible modeling framework of internal subpopulations, whose precision can be adapted to the most significant level of description, depending on the context and the questions asked.

We have also established that not only this structure matters, but also its interaction with instantaneous finite-size fluctuations of the noise and the time evolution of the *global* dynamics. These are all constitutive of the observed behaviors, and none can be neglected to understand them, which after all, is a universal feature of *complex systems*.

Also, our results showed that, for the AdEx network, there exists a time window, characterized by a high variance across noise realizations, during which it is possible to reverse the behavior by applying an appropriate stimulation. The use of a stimulus to interrupt a seizure has been applied in the past in the case of absence seizure (Rajna & Lona, 1989). These results have been used as bases of computational studies at the scale of the EEG (Taylor et al., 2014).

Computational work on the response of a network model to stimuli to disrupt seizure-like activities has shown the importance of the precise timing of the stimulation (Anderson, Kudela, Cho, Bergey, & Franaszczuk, 2007). Then, the use of electrode stimulation has been developed in rodents (Pais-Vieira et al., 2016). These different approaches have been implemented, including deep brain stimulation, vagus nerve stimulation (Boon, Cock, Mertens, & Trinka, 2018) and magnetic stimulation (Ye & Kaszuba, 2019). However, experimental recordings of the response to stimuli do not allow us to understand the mechanisms of large populations of neurons. Indeed, even if progress in calcium imaging or in multi-electrode arrays has made it possible since this last decade to record a large number of neurons simultaneously, we do not yet have access to the exact structure of the network they constitute. The study presented here is thus a proof of concept, based on a specific network model.

This said, the advantage of such a computational study is two-fold. On the one hand, linking internal structure with measured dynamics could foster more systematic interactions between experimentalists and theoreticians, with the constant goal of refining models to render them closer to reality and/or better at predicting real-life situations. On the other hand, it can shed lights on possible guidance for the design of new experimental protocols aimed at preventing the spread (or generalization) of epileptic seizures.

Generally speaking, our models describe an interesting variety of network dynamics in relation to the propagation of strong incoming perturbations. The studies on the dynamics of "crises" in networks of neuron models are a recent developing field (*Computational Neuroscience in Epilepsy*, 2008; Naze, Bernard, & Jirsa, 2015; Rich, Hutt, Skinner, Valiante, & Lefebvre, 2020; Depannemaecker et al., 2021). Another approach proposes to study computationally how a network can be stabilized by the means of an external modulatory stimulus and internal

noise, and consequently, avoid the seizure-like regime (Rich et al., 2020). They also show the specific implications of the inhibitory population. Thus recent studies are complementary to offer an understanding of the different facets of this phenomenon of seizure.

Future work should examine the large-scale consequences of these properties, and for this, it will be necessary to design macroscopic population models that capture the propagative/non-propagative aspects of the seizure, while taking into account internal heterogeneities of the network (work in progress).

References

Anderson, W., Kudela, P., Cho, J., Bergey, G., & Franaszczuk, P. (2007, 09). Studies of stimulus parameters for seizure disruption using neural network simulations. *Biological cybernetics*, *97*, 173-94. doi: 10.1007/s00422-007-0166-0

Beghi, E. (2019, December). The epidemiology of epilepsy. *Neuroepidemiology*, *54*(Suppl. 2), 185–191. Retrieved from `https://doi.org/10.1159/000503831` doi: 10.1159/000503831

Boon, P., Cock, E. D., Mertens, A., & Trinka, E. (2018, April). Neurostimulation for drug-resistant epilepsy. *Current Opinion in Neurology*, *31*(2), 198–210. Retrieved from `https://doi.org/10.1097/wco.0000000000000534` doi: 10.1097/wco.0000000000000534

Brunel, N. (2000). Dynamics of sparsely connected networks of excitatory and inhibitory spiking neurons. *Journal of computational neuroscience*, *8*(3), 183–208.

Carlu, M., Chehab, O., Porta, L. D., Depannemaecker, D., Héricé, C., Jedynak, M., ... di Volo, M. (2020, March). A mean-field approach to the dynamics of networks of complex neurons, from nonlinear integrate-and-fire

to hodgkin–huxley models. *Journal of Neurophysiology*, *123*(3), 1042–1051. Retrieved from https://doi.org/10.1152/jn.00399.2019 doi: 10.1152/jn.00399.2019

Computational neuroscience in epilepsy. (2008). Elsevier. Retrieved from https://doi.org/10.1016/b978-0-12-373649-9.x5001-7 doi: 10.1016/b978-0-12-373649-9.x5001-7

Dehghani, N., Peyrache, A., Telenczuk, B., Quyen, M. L. V., Halgren, E., Cash, S. S., ... Destexhe, A. (2016, March). Dynamic balance of excitation and inhibition in human and monkey neocortex. *Scientific Reports*, *6*(1). Retrieved from https://doi.org/10.1038/srep23176 doi: 10.1038/srep23176

Depannemaecker, D., Destexhe, A., Jirsa, V., & Bernard, C. (2021, February). Modeling seizures: From single neurons to networks. *preprint*. Retrieved from https://doi.org/10.20944/preprints202102.0478.v1 doi: 10.20944/preprints202102.0478.v1

Depannemaecker, D., Ivanov, A., Lillo, D., Spek, L., Bernard, C., & Jirsa, V. (2020, October). A unified physiological framework of transitions between seizures, sustained ictal activity and depolarization block at the single neuron level. Retrieved from https://doi.org/10.1101/2020.10.23.352021 doi: 10.1101/2020.10.23.352021

El Boustani, S., Pospischil, M., Rudolph-Lilith, M., & Destexhe, A. (2007). Activated cortical states: experiments, analyses and models. *Journal of Physiology-Paris*, *101*(1-3), 99–109.

Górski, T., Depannemaecker, D., & Destexhe, A. (2021, January). Conductance-based adaptive exponential integrate-and-fire model. *Neural Computation*, *33*(1), 41–66. Retrieved from https://doi.org/10.1162/neco$_{a0}$1342

754 doi: 10.1162/neco$_{a0}$1342

755 Hille, B. (1992). *Ionic channels of excitable membranes*. Sunderland, Mass:
756 Sinauer Associates.

757 Hodgkin, A. L., & Huxley, A. F. (1952, August). A quantitative descrip-
758 tion of membrane current and its application to conduction and ex-
759 citation in nerve. *The Journal of Physiology*, *117*(4), 500–544. Re-
760 trieved from https://doi.org/10.1113/jphysiol.1952.sp004764 doi:
761 10.1113/jphysiol.1952.sp004764

762 Jirsa, V. K., Stacey, W. C., Quilichini, P. P., Ivanov, A. I., &
763 Bernard, C. (2014, 8). On the nature of seizure dynam-
764 ics. *Brain : a journal of neurology*, *137*(Pt 8), 2210–30. Re-
765 trieved from http://www.ncbi.nlm.nih.gov/pubmed/24919973
766 http://www.pubmedcentral.nih.gov/articlerender.fcgi?artid=PMC4107736
767 doi: 10.1093/brain/awu133

768 Jiruska, P., de Curtis, M., Jefferys, J. G. R., Schevon, C. A.,
769 Schiff, S. J., & Schindler, K. (2013, January). Synchro-
770 nization and desynchronization in epilepsy: controversies and hy-
771 potheses. *The Journal of Physiology*, *591*(4), 787–797. Re-
772 trieved from https://doi.org/10.1113/jphysiol.2012.239590 doi:
773 10.1113/jphysiol.2012.239590

774 Lagarde, S., Buzori, S., Trebuchon, A., Carron, R., Scavarda, D., Milh, M., ...
775 Bartolomei, F. (2018, November). The repertoire of seizure onset patterns
776 in human focal epilepsies: Determinants and prognostic values. *Epilep-*
777 *sia*, *60*(1), 85–95. Retrieved from https://doi.org/10.1111/epi.14604
778 doi: 10.1111/epi.14604

779 Nadler, J. V., & Spencer, D. D. (2014). What is a seizure focus? , 55–62.
780 Retrieved from https://doi.org/10.1007/978-94-017-8914-1$_4$ doi:

781 10.1007/978-94-017-8914-1$_4$

782 Naud, R., Marcille, N., Clopath, C., & Gerstner, W. (2008). Firing patterns in
783 the adaptive exponential integrate-and-fire model. *Biological cybernetics*,
784 *99*(4-5), 335.

785 Naze, S., Bernard, C., & Jirsa, V. (2015, May). Computational modeling
786 of seizure dynamics using coupled neuronal networks: Factors shaping
787 epileptiform activity. *PLOS Computational Biology*, *11*(5), e1004209. Re-
788 trieved from `https://doi.org/10.1371/journal.pcbi.1004209` doi:
789 10.1371/journal.pcbi.1004209

790 Neumann, A. R., Raedt, R., Steenland, H. W., Sprengers, M., Bzymek, K.,
791 Navratilova, Z., ... Luczak, A. (2017, August). Involvement of fast-
792 spiking cells in ictal sequences during spontaneous seizures in rats with
793 chronic temporal lobe epilepsy. *Brain*, *140*(9), 2355–2369. Retrieved from
794 `https://doi.org/10.1093/brain/awx179` doi: 10.1093/brain/awx179

795 Pais-Vieira, M., Yadav, A. P., Moreira, D., Guggenmos, D., Santos, A.,
796 Lebedev, M., & Nicolelis, M. A. L. (2016, September). A closed
797 loop brain-machine interface for epilepsy control using dorsal col-
798 umn electrical stimulation. *Scientific Reports*, *6*(1). Retrieved from
799 `https://doi.org/10.1038/srep32814` doi: 10.1038/srep32814

800 Peyrache, A., Dehghani, N., Eskandar, E. N., Madsen, J. R., Anderson,
801 W. S., Donoghue, J. A., ... Destexhe, A. (2012, January). Spatiotem-
802 poral dynamics of neocortical excitation and inhibition during human
803 sleep. *Proceedings of the National Academy of Sciences*, *109*(5), 1731–
804 1736. Retrieved from `https://doi.org/10.1073/pnas.1109895109` doi:
805 10.1073/pnas.1109895109

806 Rajna, P., & Lona, C. (1989, April). Sensory stimulation for inhi-
807 bition of epileptic seizures. *Epilepsia*, *30*(2), 168–174. Retrieved

from https://doi.org/10.1111/j.1528-1157.1989.tb05450.x doi: 10.1111/j.1528-1157.1989.tb05450.x

Rich, S., Hutt, A., Skinner, F. K., Valiante, T. A., & Lefebvre, J. (2020, September). Neurostimulation stabilizes spiking neural networks by disrupting seizure-like oscillatory transitions. *Scientific Reports*, *10*(1). Retrieved from https://doi.org/10.1038/s41598-020-72335-6 doi: 10.1038/s41598-020-72335-6

Saggio, M. L., Crisp, D., Scott, J. M., Karoly, P., Kuhlmann, L., Nakatani, M., ... Stacey, W. C. (2020, July). A taxonomy of seizure dynamotypes. *eLife*, *9*. Retrieved from https://doi.org/10.7554/elife.55632 doi: 10.7554/elife.55632

Saggio, M. L., Spiegler, A., Bernard, C., & Jirsa, V. K. (2017). Fast–Slow Bursters in the Unfolding of a High Codimension Singularity and the Ultra-slow Transitions of Classes. *The Journal of Mathematical Neuroscience*, *7*(1), 7. Retrieved from https://doi.org/10.1186/s13408-017-0050-8 doi: 10.1186/s13408-017-0050-8

Taylor, P. N., Wang, Y., Goodfellow, M., Dauwels, J., Moeller, F., Stephani, U., & Baier, G. (2014, December). A computational study of stimulus driven epileptic seizure abatement. *PLoS ONE*, *9*(12), e114316. Retrieved from https://doi.org/10.1371/journal.pone.0114316 doi: 10.1371/journal.pone.0114316

Ye, H., & Kaszuba, S. (2019, December). Neuromodulation with electromagnetic stimulation for seizure suppression: From electrode to magnetic coil. *IBRO Reports*, *7*, 26–33. Retrieved from https://doi.org/10.1016/j.ibror.2019.06.001 doi: 10.1016/j.ibror.2019.06.001

Equations

Adex model:

$$C\frac{dV}{dt} = g_L(E_L - V) + g_L\Delta_T \exp\left(\frac{V - V_T}{\Delta_T}\right) - w + I_{syn} \tag{13}$$
$$\tau_w \frac{dw}{dt} = a(V - E_L) - w$$

$$\text{if } V \geq V_D \quad \text{then} \begin{cases} V \to V_R \\ w \to w + b \end{cases} \tag{14}$$

CAdEx model:

$$C\frac{dV}{dt} = g_L(E_L - V) + g_L\Delta_T \exp\left(\frac{V - V_T}{\Delta_T}\right) + g_A(E_A - V) + I_s \tag{15}$$
$$\tau_A \frac{dg_A}{dt} = \frac{\bar{g}_A}{1 + \exp\left(\frac{V_A - V}{\Delta_A}\right)} - g_A$$

(16).

$$\text{if } V \geq V_D \quad \text{then} \begin{cases} V \to V_R \\ g_A \to g_A + \delta g_A \end{cases} \tag{16}$$

HH model:

$$C_m\frac{dV}{dt} = -g_l(E_l - V) - g_K n^4(V - E_K) - g_{Na} m^3 h(V - E_{Na}) + I_{syn} \tag{17}$$

with gating variables (in ms):

$$\frac{dn}{dt} = \frac{0.032(15. - V + V_T)}{(exp(\frac{15. - V + V_T}{5.}) - 1.)}(1. - n) - 0.5exp(\frac{10. - V + V_T}{40.})n \tag{18}$$

$$\frac{dh}{dt} = 0.128exp(\frac{17. - V + V_T}{18.})(1. - h) - \frac{4.}{1 + exp(\frac{40. - V + V_T}{5.})}h \tag{19}$$

$$\frac{dm}{dt} = \frac{0.32(13. - V + V_T)}{(exp(\frac{13. - V + V_T}{4.}) - 1.)}(1 - m) - \frac{0.28(V - V_T - 40.)}{(exp(\frac{V - V_T - 40.}{5.}) - 1.)}m \tag{20}$$

Conductance-based synapses:

$$I_{syn} = g_E(E_E - V) + g_I(E_I - V) \tag{21}$$

$$\frac{dg_{E/I}}{dt} = -\frac{g_{E/I}}{\tau_{syn}} \tag{22}$$

External perturbation:

$$\begin{aligned} \nu_{pert}(t) = \beta + \alpha * (exp(-(t - T_1)^2/(2. * \tau_{on}^2)) * H(-(t - T_1)) \\ +H(-(t - T_2)) * H(t - T_1) + exp(-(t - T_2)^2/(2. * \tau_{off}^2)) * H(t - T_2)) \end{aligned} \tag{23}$$

Kuramoto order parameter:

$$R \exp i\Psi = \frac{1}{N} \sum_j \exp i\theta_j^v \tag{24}$$